

# Cannabinoids Disrupt Memory Encoding by Functionally Isolating Hippocampal CA1 from CA3

Roman A. Sandler <sup>\*1</sup>, Dustin Fetterhoff <sup>2</sup>, Robert E. Hampson <sup>2</sup>, Sam A.  
Deadwyler <sup>2</sup> & Vasilis Z. Marmarelis<sup>1</sup>

<sup>1</sup>Department of Biomedical Engineering, University of Southern  
California, Los Angeles, CA, USA

<sup>2</sup>Department of Physiology & Pharmacology, Wake Forest University,  
Winston-Salem, NC, USA

December 15, 2016

## Abstract

*Much of the research on cannabinoids (CBs) has focused on their effects at the molecular and synaptic level. However, the effects of CBs on the dynamics of neural circuits remains poorly understood. This study aims to disentangle the effects of CBs on the functional dynamics of hippocampal Schaffer collateral synapse by using data-driven nonparametric modeling. Multi-unit activity was recorded from rats doing an episodic memory task in control sessions and under the influence of exogenously administered tetrahydrocannabinol (THC), the primary CB found in marijuana. It was found that THC left firing rate unaltered and only slightly reduced theta oscillations. Multivariate autoregressive models, estimated from spontaneous spiking activity, were then used to describe the dynamical transformation from CA3 to CA1. They revealed that THC served to functionally isolate CA1 from CA3 by reducing feedforward excitation and theta information flow. The functional isolation was compensated by increased feedback excitation within CA1, thus leading to unaltered firing rates. Finally, both of these effects were shown to be correlated with memory impairments in the episodic memory task. By elucidating the circuit mechanisms of CBs, these results help close the gap in knowledge between the cellular and behavioral effects of CBs.*

Research into cannabinoids (CBs) over the last several decades has found that they induce a large variety of oftentimes opposing effects on various neuronal receptors and processes. Due to this plethora of effects, disentangling how CBs influence neuronal circuits has proven challenging. This paper contributes to this by using data driven modeling to examine how THC affects the input-output relationship in the Schaffer collateral synapse in the hippocampus. It was found that THC functionally isolated CA1 from CA3 by reducing feedforward excitation and theta information flow while simultaneously increasing feedback excitation within CA1. By elucidating the circuit mechanisms of CBs, these results help close the gap in knowledge between the cellular and behavioral effects of CBs.

---

\*Corresponding Author: rsandler00@gmail.com

## 1 Introduction

Recent years have seen a resurgence of interest in the therapeutic role of cannabinoids for several diseases and neuropsychiatric disorders such as psychosis, anxiety disorders, PTSD, and multiple sclerosis [1, 2]. Their role in epilepsy, in particular has attracted a lot of somewhat controversial attention as various types of cannabinoids at various doses have been shown to be both pro- and anticonvulsant [3, 4, 5, 6, 7, 8, 7]. Parallel to increasing therapeutic research, much work has been done on the chemical structure of various cannabinoids, cannabinoid receptors, along with their cellular interactions and pharmacology [9].

Nonetheless, between the large bodies of literature on cannabinoids from chemical, disease, and behavioral perspectives, much less work has been done to explore the effects of cannabinoids on the neural circuit level. This is particularly important since a wide range of complex and often opposing effects have been attributed to cannabinoids on a molecular and cellular level. For example, cannabinoid activation of CB1 receptors, which are found on both pyramidal cells and interneurons, reduces the quantity of neurotransmitter released during an action potential; consequently, increased extracellular cannabinoid levels reduce both excitatory (glutamatergic) and inhibitory (GABAergic) transmission [10]. Furthermore, cannabinoids have been shown to interact with astrocytes [11], mitochondria [12], glycine receptors [13], vanilloid receptors [14], and reduce GABA and glutamate reuptake [15, 16]. Consequently, it is very difficult to extrapolate the emergent network level changes simply from a catalogue of effects cannabinoids have a cellular/molecular level.

Here, we studied the effects of  $\Delta^9$ -tetrahydrocannabinol (THC) on hippocampal networks during memory encoding using spiking activity recorded in rodents in-vivo performing the Delayed-NonMatch-to-Sample (DNMS) episodic memory task. Multivariate autoregressive (MVAR) models [17], were used in both control and THC sessions to estimate feedforward and feedback dynamical filters, which are akin to the waveform shapes of the CA3→CA1 EPSP and CA1 afterhyperpolarization, respectively. MVAR models, which are a type of linear nonparametric models, are 'data-driven' in the sense that they estimate model parameters directly from recorded neural spiketrains and, unlike more biologically realistic models, make very few *a priori* assumptions on the nature of the neural dynamics [18, 19]. This makes them particularly well suited for this study, since as previously mentioned the emergent effects of THC on neural circuits is highly complex and unclear. Overall our results suggest that cannabinoids impair memory encoding by functionally isolating CA1 from CA3 via reduced theta information flow and altered excitatory-inhibitory balance across the Schaffer collateral synapse.

## 2 Results

### 2.1 Changes in rate and temporal coding under Cannabinoids

To evaluate the effects of exogenous cannabinoids on the hippocampal network 1 mg/kg THC was injected intraperitoneally into  $N = 6$  rodents during certain sessions while they were performing a DNMS task (Fig. 6). All data was previously used in a study on the effects of cannabinoids on hippocampal multifractality [20, 21]. Briefly, in the sample phase, the rats were presented one of two levers. After a variable length delay, both levers were presented in the match phase and the rat had to choose the opposite lever to receive a reward. On the behavioral level, it was found that THC impaired rodent-performance on the DNMS task by about  $12.2 \pm .6\%$  (Fig. 1a, Hampson and Deadwyler [22]).

While performing the DNMS task single-unit activity was recorded from the hippocampal CA3 and CA1 regions using a multi-electrode array. No mean firing rate (MFR) changes were seen during THC sessions in either CA3 or CA1 cells ( $P=.502$ , Fig. 1b). This includes activity around the DNMS sample phase, during the entire session, and in both general cells and sample-presentation cells (see below). The lack of any cannabinoid-induced changes in firing rates at this dosage has been observed in previous studies [23, 24].

Two types of temporal coding were identified in the recorded spiketrains. First, on slower timescales, several neurons fired preferentially in response to lever presentation in the sample phase of the DNMS task. These sample-presentation cells are a subtype of the functional cell types (FCTs) described previously [25]. It was found that THC reduced the proportion of sample-presentation cells in both CA3 and CA1 by roughly equal amounts ( $\Delta = 13 \pm 4\%$ ,  $P < .001$ ; Fig. 1c). Interestingly, some sample-presentation cells lost all of their preferential firing in THC sessions (Fig.1d); this contrasts with place cells whose receptive field stays largely intact under cannabinoids [26]. There was an interesting but insignificant trend connecting sample-presentation cell reduction with behavioral deficits ( $R^2 = .27$ ,  $P = .052$ , Fig. 8a).

On faster timescales, it was found that several CA3 and CA1 neurons had theta band rhythmicity (4-7 Hz). Hippocampal theta oscillations are known to be intimately related to cognitive function [27, 28, 29] and have previously been linked to performance in the DNMS task [30]; furthermore, theta oscillations are known to be reduced by systemic injections of cannabinoids on both the single unit [23] and network level [31]. It was found that CA1 theta power was slightly but significantly reduced in THC sessions ( $\Delta = 2.52\%$ ,  $CI : [.61, 4.4]\%$   $P = .004$ ; Fig. 1e). A similar, albeit slightly weaker, theta power reduction was seen in CA3 cells ( $\Delta = 1.94\%$ ,  $P = .045$ ; Fig. 7). Unlike previous results in a different task [23], the reduction in CA1 theta power was not found to be correlated with behavioral deficits in the DNMS task ( $P = .674$ , Fig. 8b).

Overall, these results show that THC has minor effects on the actual neuronal spiketimes: quantity of spikes (MFR) was not affected and spike rhythmicity (theta oscillations) were only slightly affected. Furthermore behavioral deficits induced by cannabinoids could not be explained by any of these factors, which are the traditional markers of rate and temporal coding in the hippocampus.

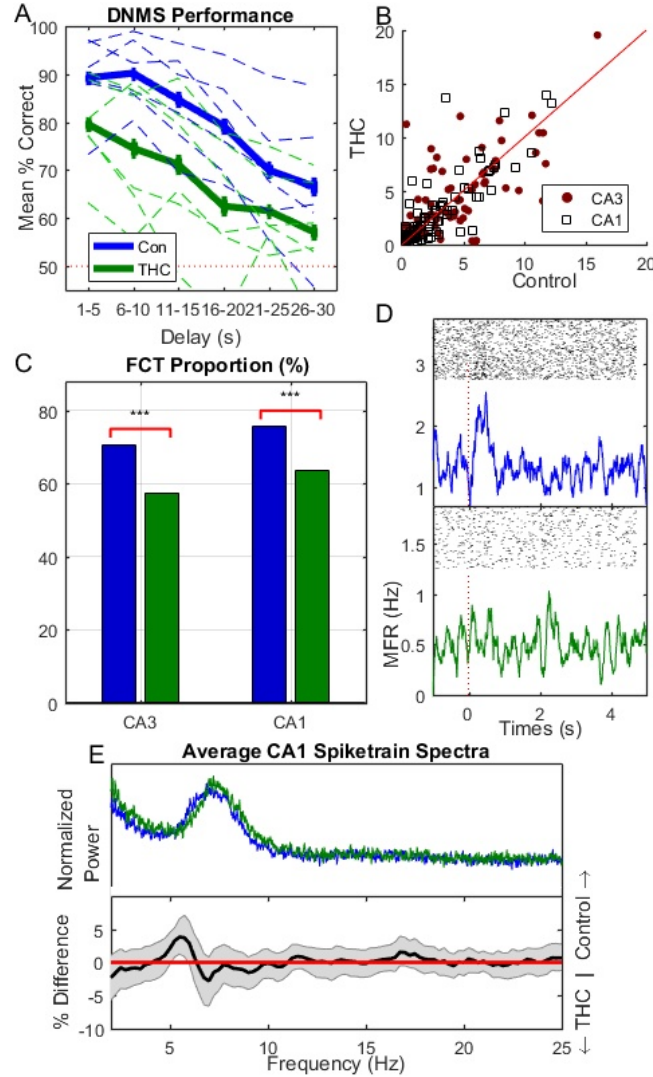


Figure 1: (A) Behavioral performance on DNMS task in both control and THC sessions. Dashed lines show individual animal performance, while solid lines show mean performance over all animals. Bars indicate SEM. Dashed red line indicates performance at chance level. (B) Individual neuron MFR. (C) Sample-presentation cell proportion in CA3 and CA1 cells in control & THC sessions (D) Example of a sample-presentation cell in a control session (top) which lost its firing specificity under THC (bottom). X-axis shows MFR (Hz) (E) Average CA1 spiketrain spectra (top). Bottom shows mean difference in individual cell spectra (thus it is not simply the difference between the signals in above which are averaged over whole population). Gray error bounds indicate 99% confidence bounds. In (B) and (E), only neurons recorded in at least one control & THC session were included. Results for neurons recorded in several control or THC sessions were averaged over those sessions.

## 127 2.2 Systems Analysis

128 The remainder of the study will focus on systems analysis of the Schaffer col-  
 129 lateral synapse connecting CA3 to CA1, and how this synapse is affected by

THC. Systems analysis aims to identify the input-output "blackbox" by which the input spiketrains are transformed into the output spiketrain. On a more abstract level, it aims to identify how the information encoded in CA3 is propagated into CA1. This is distinct from the *signal* analysis done in the previous section which only looks at features of individual spiketrains rather than the causal relationship between multiple spiketrains as done in systems analysis.

The relationship between an arbitrary number of input CA3 spiketrains and the output CA1 spiketrain was modeled using a multivariate autoregressive model described by Eq. 1 and an example of which is pictured in Fig. 2a. Each system consists of  $N$  input CA3 neurons and  $N$  feedforward filters describing the dynamical input-output relationship between the given CA3 and CA1 neurons. Intuitively, these filters can be thought of as the EPSP elicited in the output CA1 neuron in response to an action potential (AP) in the input CA3 neuron. However, unlike EPSPs which traditionally only encapsulate ion-conductances from neurotransmitter-gated ion channels, the "blackbox" nature of the feedforward filters means they also include more complex dynamical effects such as dendritic integration, spike generation, active membrane conductances, and feedforward interneuronal inhibition (thereby allowing the filters between two pyramidal cells to be inhibitory). Each model also includes an feedback (autoregressive) filter which describes the effects of past output spikes onto the output present. This filter, which can be intuitively thought of as the afterhyperpotential (AHP) [32] includes intracellular processes such as the absolute and relative refractory period, slow potassium conductances, and  $I_h$  conductances. It also includes more complex intercellular processes such as the recurrent connections between CA1 pyramidal cells and interneurons [33]. Neuronal connectivity was estimated using a stepwise input selection procedure. Filter parameters were estimated using the Laguerre expansion technique and least-squares regression using neuronal activity around the sample phase. Model significance was verified using ROC plots and shuffling methods (see supplementary methods).

A representative connectivity grid from a recorded THC session with 10 recorded neurons (4 CA3, 6 CA1) is shown in Fig. 2a. Fig. 2b shows a sample system from this session between 3 CA3 pyramidal cells and 1 CA1 pyramidal cell. Note that two of the feedforward filters are excitatory (above the x-axis) while the third has both excitatory and inhibitory components, presumably arising through feedforward inhibition involving interneurons [34, 35]. The system also involves a feedback filter which shows a relatively long refractory period ( $\sim 40$ ms) followed oscillatory bursting activity. Oscillations in the CA1 pyramidal cell AHP are a well known phenomena caused by slow  $K^+$  and  $I_h$  conductances, and these oscillations are known to lead to theta resonances [36, 37, 17]. In order to study the filter oscillations more closely, the filter frequency spectra were plotted in Fig. 2c. Both feedforward excitatory filters were found to have peaks in the high theta range (8-9 Hz). Intuitively, this can be understood to mean that information encoded in the theta range in these input neurons is preferentially transmitted to the output CA1 neuron. Furthermore, the feedback filter has a low theta resonance of 3.5 Hz. Significance metrics for the displayed system is shown in Supp. Fig. 9, and additional systems are shown

176 in Supp. Fig. 10. All together 66% (707/1068) of all systems were found to be  
 177 significant and 2139 feedforward and 707 feedback filters were obtained. THC  
 178 was found to reduce the amount of significant models per session ( $\Delta = -7.4\%$ ,  
 179  $P = .011$ ), but the predictive power of significant models, as measured by AUC  
 180 (see supplementary methods), was unaltered ( $P = .24$ ).

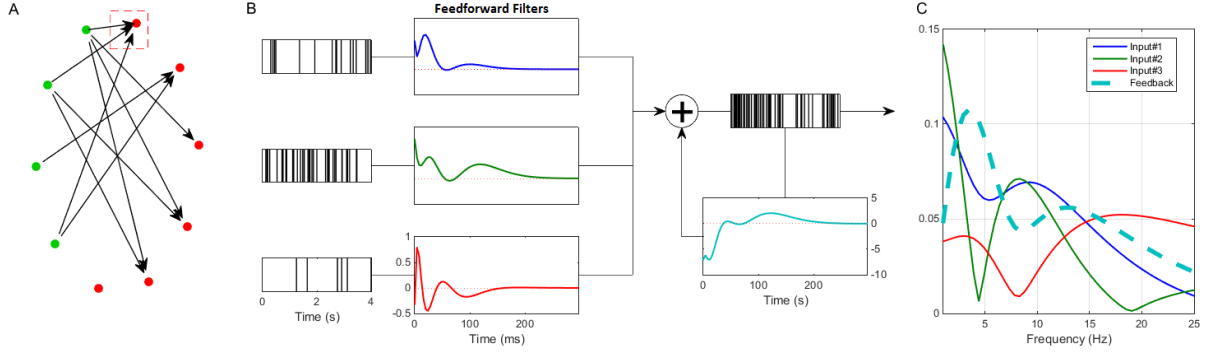


Figure 2: (A) Example connectivity grid of 4 CA3 neurons (green) and 6 CA1 neurons (red) recorded during a single session. Note that 1 CA1 neuron has no significant inputs. Each line represents a causal connection between those neurons, as encapsulated by a feedforward filter. (B) Example system of CA1 neuron enclosed by the red box in (A). Diagram shows 3 input CA3 spiketrains followed by their respective feedforward filters which are summed with the feedback filter to generate the output CA1 spiketrain. All feedforward filter are plotted with the same y-axis scale. Dashed red line in filter boxes indicates x-axis. (C) Normalized filter spectra computed of feedforward and feedback filters from (B).

181 To study how THC affects system dynamics on a population level, we ex-  
 182 amined how features change in the entire sample of control and THC filters.  
 183 The average filter frequency profile for both control and THC sessions is shown  
 184 in Fig. 3a,b (top). Both feedforward and feedback spectra are found to have  
 185 clear theta band peaks, thus generalizing the trend seen in the example system  
 186 of Fig. 2. This confirms previous reports which show that CA3 propagates  
 187 strong theta rhythms to CA1 [38, 39] and also that CA1 is capable of generating  
 188 endogenous theta rhythms [40]. A significant decline was found in the theta  
 189 power of the feedback filters ( $\Delta = 20.8\%$ ,  $P < .001$ ; Fig. 3b). Note that the  
 190 feedback filter theta reduction is about 10x stronger than the theta reduction  
 191 found in the CA1 spiketrain signals (Fig. 1e. No reduction in theta power was  
 192 found in the feedforward filters ( $P = .61$ , Fig. 3a). This surprising result sug-  
 193 gests that cannabinoid-induced theta desynchronization results primarily from  
 194 altered feedback properties rather than changes in CA3→CA1 dynamics.

195 Cannabinoids have been reported to affect network excitation-inhibition bal-  
 196 ance (EIB) [10, 41]. Particularly, there is much debate whether cannabinoids are  
 197 pro- or anticonvulsants [8, 42, 43, 4, 6]. In order to examine the effects cannabi-  
 198 noids have on network EIB, we quantified the excitation of the estimated filters  
 199 using a metric called the excitatory index (EI), which is the ratio between posi-  
 200 tive filter area and total filter area. It was found that THC had no significant  
 201 effect on feedforward EI ( $P = .14$ ); however, there was an interesting but in-

202 significant trend showing that THC-induced decreases in feedforward EI were  
 203 correlated with behavioral deficits ( $R^2 = .27, P = .063$ , Fig. 3c). Additionally,  
 204 THC reduced the amount of casually connected CA3-CA1 neuronal pairs  
 205 ( $\Delta = -8.9\%$ ,  $P < .001$ ). These findings, together with the THC-induced de-  
 206 crease of CA3→CA1 significant models, suggest that THC reduces the causal  
 207 influence CA3 neurons have on CA1 spiketimes. In other words, THC can be  
 208 said to functionally isolate CA1 from CA3. It was also found that THC sig-  
 209 nificantly increased feedback EI ( $\Delta = 3.5\%$ ,  $P = .022$ ) and that the increased  
 210 feedback EI was correlated with behavioral deficits ( $R^2 = .38, P = .007$ , Fig.  
 211 3d). Essentially, the more THC increased feedforward inhibition and feedback  
 212 excitation, the worse the rodent did on the task.

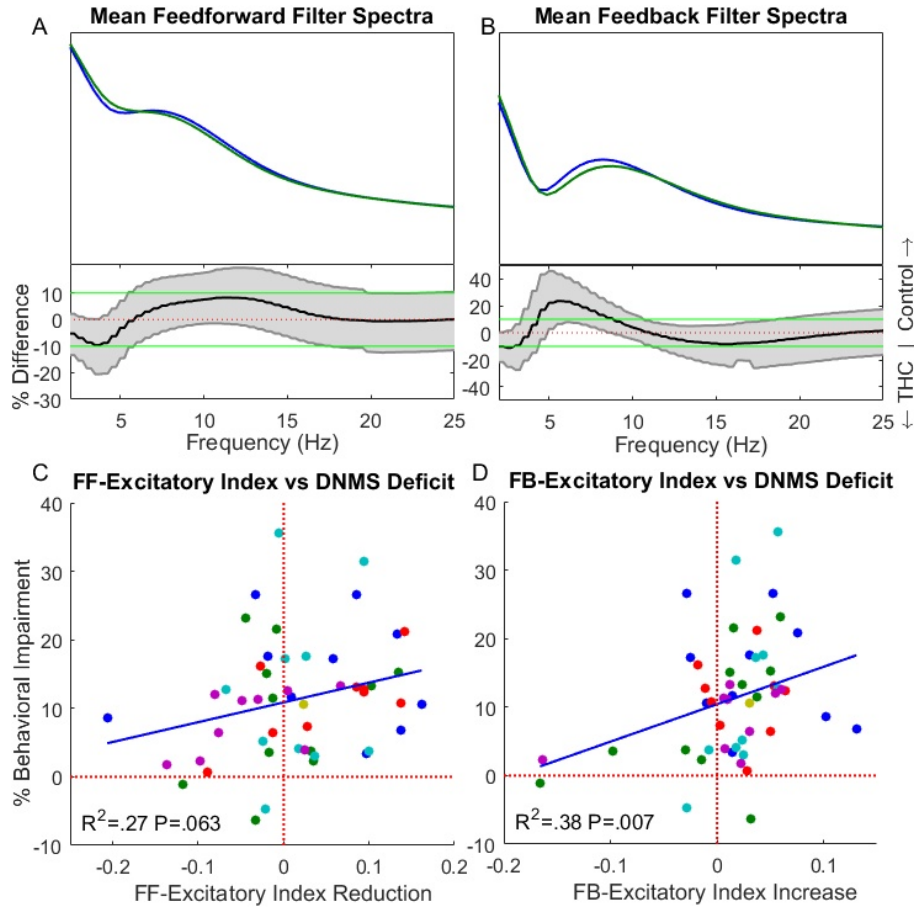


Figure 3: Average feedforward (A) and feedback (B) filter spectra in control and THC sessions (top), and their differences (bottom). Same format and analysis as Fig. 1a. (C) Correlation between feedforward filter EI reduction and behavioral deficits. Each point represents a specific THC session, with points of the same color coming from the same animal. X-axis (Y-axis) shows reduction in feedforward EI (behavioral performance level) from mean control levels (see supplemental methods) (D) Same as (C) but for feedback EI increase.

## 2.3 PDM Analysis

The large quantity ( $>2800$ ) and variability of the obtained filters describing the CA3→CA1 dynamic transformation presents a challenge of interpretation. Namely, how could one identify features from the entire filter population which are representative of the CA3→CA1 transformation rather than just the input-output relationship found in this or that particular pair of neurons. In essence this is an unsupervised learning problem which aims to identify hidden structure within the filter population for the purpose of knowledge discovery. Our group has developed the concept of the global principal dynamic modes (gPDMs) towards this effort [18, 44, 45]. The gPDMs are a system-specific and efficient basis set which contain the essential dynamic components of the filter population and are meant to be amenable to biological interpretation. One set of gPDMs were estimated from all (control and THC) obtained filters with the hypothesis that THC would primarily change the expression strength of the gPDMs rather than their specific shapes.

Fig. 4a,b shows the obtained feedforward and feedback gPDMs in both the time and frequency domain. Once again, the feedforward and feedback gPDMs represent the dominant independent components of feedforward and feedback kernels, respectively. The first, and thus most significant, feedforward gPDM was found to have almost all its energy in the 1st time bin, with an immediate decline thereafter. This gPDM represents near concurrent firing between CA3 and CA1 neurons and presumably results from both direct CA3→CA1 connections via the Schaffer collateral synapse [46, 47] and common inputs from the entorhinal cortex [48, 49]. The third feedforward gPDM, which is characterized by an initial inhibitory phase, presumably represents feedforward interneuronal inhibition which is prevalent in the CA3→CA1 connection [34, 35]. THC was not found to influence the strength of either of these gPDMs ( $P = .76$ ,  $P = .60$ ; Fig. 11). The second feedforward gPDM which is characterized by sustained and oscillatory excitation was found to have a strong theta peak in the frequency domain. Furthermore, it was found that THC-induced declines in the strength of this gPDM were correlated with behavioral deficits ( $R^2 = .30$ ,  $P = .032$ ; Fig. 4c).

The three obtained feedback gPDMs are shown in Fig. 4b. These gPDMs express the essential feedback dynamics found in CA1 neurons. As previously mentioned, these dynamics arise through the combination of intracellular processes such as the AHP and extracellular processes such as recurrent connections between CA1 pyramidal cells and interneurons. It was found that THC-induced increases in the third feedback gPDM were correlated with behavioral deficits ( $R^2 = .39$ ,  $P = .005$ ; Fig. 4d). This correlation was not seen in either of the first two feedback gPDMs ( $P = .32$ ,  $P = .75$ ; Fig. 11). Notably, the 3rd feedback gPDM was seen to be "theta-blocking" in the frequency domain - namely, it serves to counteract the 1st "theta-promoting" feedback gPDM and disrupts theta oscillations in the CA1 neuron. The THC-induced changes in the feedforward and feedback theta gPDMs paint a more complete picture of the CA1 theta reductions seen in Fig. 1e. Namely, they attribute the theta losses to spe-



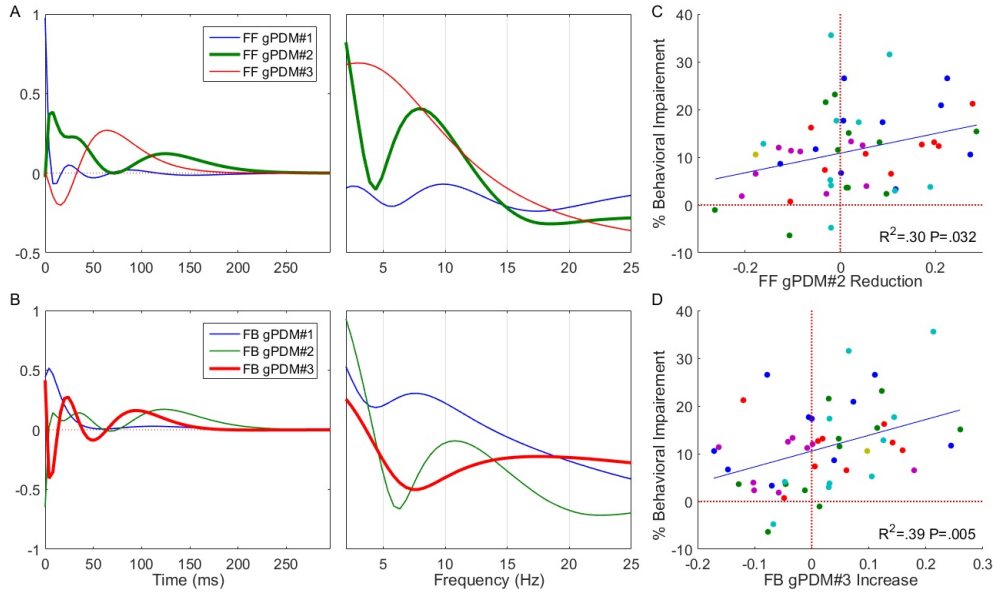


Figure 4: Feedforward (A) and feedback (B) gPDMs in both the time (left) and frequency domain (right). Reductions in 2nd feedforward gPDM (C) and increases in 3rd feedback gPDM (D) were found to be correlated with behavioral deficits. Same format as Fig. 3.

258 cific feedforward and feedback dynamical filters which may potentially be traced  
 259 to specific biophysical mechanisms. Furthermore, changes in these dynamical  
 260 filters have been specifically correlated with behavioral deficits, which could not  
 261 be done with theta reductions in the CA1 signal (Fig. 8).

### 262 3 Discussion

263 The current study uses 'data-driven' nonparametric system dynamics modeling  
 264 tools to study the effects of THC on the Schaffer Collateral synapse in rodents.  
 265 The chief findings of the study can be summarized as: (1) THC induced little  
 266 or no change in traditional rate and temporal coding metrics such as MFR and  
 267 theta power, (2) THC altered the CA1 excitatory-inhibitory balance by reducing  
 268 feedforward influence from CA3 while increasing feedback excitation from CA1,  
 269 (3) THC reduced theta information flow through the Schaffer collateral synapse,  
 270 and (4) The magnitudes of both of the previous effects were directly correlated  
 271 with the severity of behavioral deficits induced by THC. Overall these results  
 272 suggest the conclusion that THC impairs memory encoding by functionally iso-  
 273 lating CA1 from CA3.

274 From a computational perspective, The nonparametric modeling methods  
 275 used in the study proved successful in studying the network level effects of  
 276 cannabinoids since, unlike biophysical models, all model parameters were es-  
 277 timated directly from recorded data and very few *a priori* assumptions were  
 278 made about the effects of THC [18, 19, 50]. The global principal dynamic modes  
 279 (gPDMs), which were derived from MVAR filters of the entire population of neu-  
 280 rons, further extracted hidden dynamical structure from 'noisy' neuron-neuron

281 variability. Importantly, THC-induced changes in the gPDMs were directly cor-  
282 related with behavioral impairments, thus justifying their utility. Furthermore,  
283 while most in-vivo studies on THC analyze macro level signals such as ECoG  
284 and EEG, this work adds to a relatively small body of literature which ana-  
285 lyzes the effects of THC on neuronal population spiking activity. Finally, to our  
286 knowledge, this is the first work which examines the effect of THC on neuronal  
287 systems dynamics, or the causal interactions between signals, rather than on  
288 neuronal signals themselves.

289 It was found that THC reduces the amount of casually connected CA3-CA1  
290 neuronal pairs; furthermore there was an interesting but insignificant trend for  
291 THC-induced deficits in feedforward excitation to lead to behavioral deficits.  
292 This trend may prove to be significant given a higher sample size. We hypoth-  
293 esize that this reduced feedforward influence is caused by decreased glutamate  
294 release from CA3 principal cells due to CB1 receptor activation by THC [51]. The  
295 reduced feedforward excitation was compensated by increased feedback excita-  
296 tion - an effect which was also correlated with behavioral deficits. We hypothesize  
297 that this is due to decreased drive from CA1 cholecystokinin (CCK)-containing  
298 basket cells. While CCK cells only make up only 13.9% of interneurons [52],  
299 they express significantly more CB1 receptors than any other cell in the hip-  
300 pocampus [53], and their primary input and output is from/to CA1 pyramidal  
301 cells [52]. Increased THC concentrations would reduce CCK output by (1) re-  
302 ducing the amount of GABA they release per action potential and (2) reducing  
303 their total amount of action potentials due to reduced glutamatergic input from  
304 CA1 pyramidal cells. Altogether, this would amount to a functional isolation, or  
305 breakdown in information flow from CA1 from CA3, thus inducing the behav-  
306 ioral impairments seen in the DNMS task. Furthermore, the only reason that  
307 MFR remained constant is that at the given dosage there was a net balance  
308 between these two opposing phenomena.

309 The 'functional isolation' hypothesis is further supported by previous work  
310 which showed that the behavioral impairments caused by cannabinoids in the  
311 DNMS task were similar to those seen with a full pharmacological lesion of the  
312 hippocampus [54]. Given the centrality of CA3→CA1 information flow to hip-  
313 pocampal function, a functional isolation of these areas could indeed presumably  
314 lead to impairments similar to that of a full lesion. Also relevant is a study by  
315 Goonawardena et al. [24] where THC was injected intraperitoneally at low 1  
316 mg/kg doses as in this study and in higher doses of 3 mg/kg. It was found  
317 that while both doses disrupted hippocampal synchrony, only the higher dose  
318 resulted in a reduction in pyramidal cell MFR. This suggests that at the lower  
319 doses both previously described phenomena are at a net balance, while at the  
320 higher dose, the decrease in feedforward excitation overpowers the increase in  
321 feedback excitation and results in lower MFR. Finally, the hypothesis predicts a  
322 breakdown in the normal spiketime coordination between pyramidal cells and in-  
323 terneurons in CA1 circuits. The breakdown of this coordination, which has been  
324 extensively implicated in hippocampal oscillations [55, 56], could be responsible  
325 for the observed decrease in theta oscillations and information flow.

326 Although the current results only suggest this hypothesis, several experi-

327 ments could be done to further substantiate it. Feedforward and feedback ker-  
328 nels and gPDMs could be estimated at different doses of THC; the hypothesis  
329 would predict that different doses would effect the two processes independently,  
330 with either of the two processes potentially being more dominant at different  
331 THC levels. Also significant developments in in-vivo synaptic patch clamping  
332 [57] and optogenetics in recent years could be used to directly measure the drive  
333 of CCK cells and CA3 pyramidal cells onto CA1 pyramidal cells under THC.

334 Much research has been done investigating the effects THC and other cannabi-  
335 noids have on seizures and epilepsy. Results so far have been mixed, with various  
336 studies showing that THC is both pro- and anticonvulsant [3, 4, 5, 6, 7, 8, 7].  
337 The results from this study and the presented hypothesis suggest that THC in-  
338 herently is not pro- or anti-convulsant but that its effects will depend on the  
339 dosage and the unique circuitry of every epileptic focus. Interestingly, a study  
340 by Rudenko et al. [6] has shown that indeed the effects of a CB1 agonist were  
341 dose dependant, with *lower* doses being anticonvulsant and higher doses being  
342 proconvulsant. Finally, study suggests that in order to truly understand the  
343 effects of THC on epileptic circuits, one must study the systems level changes  
344 in circuit dynamics rather than taking a reductionist approach and studying the  
345 effects of THC on any particular receptor or cell type.

346 The present study analyzed the effects of THC from both a signals and sys-  
347 tems perspective - and found that systems analysis yielded much richer results.  
348 For example, while analysis of CA1 spiketrain signals showed a slight (2%) re-  
349 duction in theta frequency, analysis of system kernels showed that the theta loss  
350 was primarily due to CA1 feedback dynamics whose kernels lost over 20% of their  
351 theta power, while theta power in feedforward kernels was unaffected. Further-  
352 more, only systems analysis allows one to analyze predictive power, feedforward  
353 and feedback excitation, and EPSP and AHP waveform shape. Notably, the  
354 finding that feedforward influence decreased while feedback excitation increased  
355 could not have been observed using only signal analysis which would have only  
356 detected a constant MFR.

357 The present study also employed gPDMs as a means to extract the most  
358 significant information from the kernel dynamics estimated from several animals  
359 over several sessions [18, 58, 17, 47]. The utility of the gPDM method was justi-  
360 fied by the finding that reductions in theta related gPDMs in a given session were  
361 directly correlated with behavioral deficits, showing that the gPDMs can isolate  
362 the particular dynamics which are most affected by THC. Furthermore, THC-  
363 induced theta power losses in spiketrain signals were not found to be correlated  
364 with behavioral deficits. Although in the present study, kernels and gPDMs were  
365 restricted to being linear in order to more easily quantify their overall strength  
366 and excitation (via the EI), future work will aim to identify the effects of THC  
367 on hippocampal nonlinear dynamics [59, 50].

## 368 Ethics Statement

369 All animal protocols were approved by the Wake Forest University Institutional  
370 Animal Care and Use Committee, in accordance with the Association for Assess-

ment and Accreditation of Laboratory Animal Care and the National Institute of Health Guide for the Care and Use of Laboratory Animals (NIH Publication No. 8023).

## Acknowledgements

This work was supported by NIH (www.nih.gov) grant P41-EB001978 to the Biomedical Simulations Resource at the University of Southern California.

## 4 Methods

### 4.1 Experimental Procedures

N=6 Male Long-Evans rats were trained to criterion on a two lever, spatial Delayed NonMatch-to-Sample (DNMS) task (see Fig. 6). Briefly, during the sample phase the rat was presented one of two levers (left or right). After a delay phase ranging from 1-30 seconds, the rat was presented both levers and had to choose the opposite level in order to attain a reward. Each rodent underwent 16-25 sessions of the task, which were roughly evenly divided between control and THC sessions, wherein the rodent was intraperitoneally administered 1 mg/kg of body weight  $\Delta^9$ -tetrahydrocannabinol (THC), an exogenous cannabinoid found in marijuana. During the task, spike trains were recorded in-vivo with multi-electrode arrays implanted in the left and right CA3 and CA1 regions of the hippocampus. In an effort to acquire a consistent cognitive state, only spiking activity around the sample phase of the task was used. Spikes from multiple trials were sorted, time-stamped, and concatenated into a discretized binary time series using a 4ms bin. For more details on the experimental setup, see supplementary methods.

### 4.2 Model Configuration and Estimation

Nonparametric multiple-input linear autoregressive models were used to model the dynamical transformation between input and output spike trains (see Fig. 2,5) [17, 50]. Each model consisted of a feedforward component, reflecting the effect of the  $N$  input cells on the output cell and a feedback (autoregressive) component reflecting the subthreshold and suprathreshold effects the output cell has on itself. Thus, the output  $y(t)$  is calculated as:

$$y(t) = \sum_{n=1}^N \sum_{\tau=0}^M k_n(\tau) x_n(t - \tau) + \sum_{\tau=1}^{M+1} k_{AR}(\tau) y(t - \tau) \quad (1)$$

where  $k_n$  reflects the feedforward filter of input  $x_n(t)$ , and  $k_{AR}$  reflects the feedback filter. In order to reduce the amount of model parameters and thereby increase parameter stability, we applied the Laguerre expansion technique to expand the feedforward and feedback filters over  $L$  Laguerre basis functions (see supplementary methods).

Effective connectivity between neurons was assessed using a Granger causality-like approach. For each output CA1 neuron, input CA3 neurons were selected in a forward stepwise procedure whereby only neurons which help predict the output CA1 spike activity were included in the model. After all input neurons were selected, a Monte Carlo approach was used to assess model significance. A model was deemed significant if the CA3 inputs could predict the output CA1 activity significantly better ( $P < .0001$ ) than randomly permuted versions of the inputs. See supplementary methods for more details.

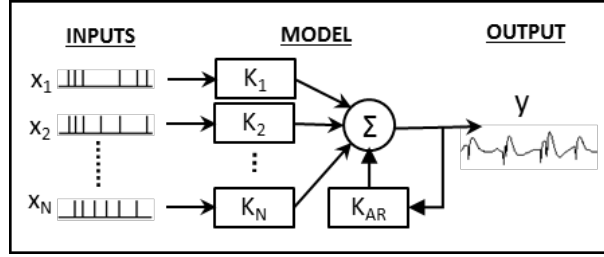


Figure 5: Model Configuration. Each model has  $N$  point-process inputs which each go through a linear filter,  $K_i$ . These inputs are then summed with the output of the feedback filter,  $K_{AR}$  to generate the final output,  $y(t)$ , which is a continuous signal

### 4.3 Principal Dynamic Modes

The global principal dynamic modes (gPDMs) were obtained in a two step process: first, all filters of each input from every animal were concatenated in a rectangular matrix. Then singular value decomposition (SVD) was performed on the rectangular matrix to obtain all the significant singular vectors, which are the gPDMs. It was found that 3 gPDMs were sufficient to describe the linear dynamics both the population of feedforward and feedback filters. gPDM strength in a given filter was computed by taking the dot product between the gPDM and the filter. gPDM strength in a given session was computed by taking the average gPDM strength in every filter of that session.

## A Supplementary Methods

All data was previously used in a study on the effects of cannabinoids on hippocampal multifractality [20, 21])

### A.1 Animals

Subjects were Long-Evans rats (Harlan) aged 4–6 months ( $n = 6$ ) individually housed and allowed free access to food with water regulation to maintain 85% of ad libitum body weight during testing. All animal protocols were approved by the Wake Forest University Institutional Animal Care and Use Committee, in accordance with the Association for Assessment and Accreditation of Laboratory Animal Care and the National Institute of Health Guide for the Care and Use of Laboratory Animals (NIH Publication No. 8023).

## 435 A.2 Apparatus

436 The behavioral testing apparatus for the delayed nonmatch-to-sample (DNMS)  
437 task is the same as reported in other studies [22] and consisted of a 43x43x50 cm  
438 Plexiglas chamber with two retractable levers (left and right) positioned on either  
439 side of a water trough on the front panel. A nosepoke device (photocell) was  
440 mounted in the center of the wall opposite the levers with a cue light positioned  
441 immediately above the nosepoke device. A video camera was mounted on the  
442 ceiling and the entire chamber was housed inside a commercially built sound-  
443 attenuated cubicle.

## 444 A.3 DNMS Task

445 The DNMS task consisted of three main phases: Sample, Delay and Nonmatch.  
446 The sample phase initiated the trial when either the left or right lever was  
447 extended (50% probability), requiring the animal to press it as the Sample Re-  
448 sponse (SR). The lever was then retracted and the Delay phase of the task  
449 initiated, as signaled by the illumination of a cue light over the nosepoke pho-  
450 tocell device on the wall on the opposite side of the chamber. At least one  
451 nosepoke (NP) was required following the delay interval which varied randomly  
452 in duration (1-30 s) on each trial during the session. The Nonmatch phase began  
453 when the delay timed out, the photocell cue light turned off and both the left  
454 and right levers on the front panel were extended. Correct responses consisted  
455 of pressing the lever in the Nonmatch phase located in the spatial position op-  
456 posite the SR (nonmatch response: NR). This produced a drop of water (0.4  
457 ml) reward in the trough between the two levers. After the NR the levers were  
458 retracted for a 10.0 second intertrial interval (ITI) before the next Sample lever  
459 was presented to begin the next trial. A lever press at the same position as the  
460 SR (match response) constituted an “error” with no water delivery and turned  
461 off of the chamber house lights for 5.0s and the next trial was presented 5.0 s  
462 later. Individual performance was assessed as % NRs (correct responses) with  
463 respect to the total number of trials (80-100) per daily (1 hr) sessions.

## 464 A.4 Drug Preparation & Administration

465  $\Delta^9$ -tetrahydrocannabinol (THC) was obtained from the National Institute on  
466 Drug Abuse as a 50 mg/ml solution in ethanol. Detergent vehicle was pre-  
467 pared from Pluronic F68 (Sigma, St. Louis, MO), 20 mg/ml in ethanol. THC  
468 was added to the detergent-ethanol solution (0.5 ml of either THC), and then 2.0  
469 ml of saline (0.9%) was slowly added to the ethanol-drug solution. The solution  
470 was stirred rapidly and placed under a steady stream of nitrogen gas to evapo-  
471 rate the ethanol (~10 min). This resulted in a detergent-drug suspension (12.5  
472 mg/ml THC), which was sonicated and then diluted with saline to final injec-  
473 tion concentrations (0.5-2.0 mg/ml THC). On drug administration days, animals  
474 were injected intraperitoneally with the drug-detergent solution (1 mg/kg) ~10  
475 min before the start of the behavioral session. Our experience with these ex-  
476 periments has shown that performance after vehicle injection is not significantly

different than no injection, and therefore was omitted during this series of experiments to minimize risk of infection to the animals. At least two no injection days were imposed between each drug-testing session. All drug solutions were mixed fresh each day.

## A.5 Surgery

All surgical procedures conformed to National Institutes of Health and Association for Assessment and Accreditation of Laboratory Animal Care guidelines, and were performed in a rodent surgical facility approved by the Wake Forest University Institutional Animal Care and Use Committee. After being trained to criterion performance level in the DNMS task animals were anesthetized with ketamine (100 mg/kg) and xylazine (10 mg/kg) and placed in a stereotaxic frame. Craniotomies (5mm-diameter) were performed bilaterally over the dorsal hippocampus to provide for implantation of 2 identical array electrodes (Neuroline, New York, NY), each consisting of two rows of 8 stainless steel wires (diameter: 20  $\mu\text{m}$ ) positioned such that the geometric center of each electrode array was centered at co-ordinates 3.4 mm posterior to Bregma and 3.0 mm lateral (right or left) to midline [60]. The array was designed such that the distance between two adjacent electrodes within a row was 200  $\mu\text{m}$  and between rows was 400  $\mu\text{m}$  to conform to the locations of the respective CA3 and CA1 cell layers. The longitudinal axis of the array of electrodes was angled 30° to the midline during implantation to conform to the orientation of the longitudinal axis of the hippocampus, with posterior electrode sites more lateral than anterior sites. The electrode array was lowered in 25-100  $\mu\text{m}$  steps to a depth of 3.0 - 4.0 mm from the cortical surface for the longer electrodes positioned in the CA3 cell layer, leaving the shorter CA1 electrodes 1.2 mm higher with tips in the CA1 layer. Extracellular neuronal spike activity was monitored from all electrodes during surgery to maximize placement in the appropriate hippocampal cell layers. After placement of the array the cranium was sealed with bone wax and dental cement and the animals treated with buprenorphine (0.01–0.05 mg/kg) for pain relief over the next 4-6 hrs. The scalp wound was treated periodically with Neosporin antibiotic and systemic injections of penicillin G (300,000 U, intramuscular) were given to prevent infection. Animals were allowed to recover from surgery for at least 1 week before continuing behavioral testing [61].

## A.6 Electrophysiological Monitoring & Preprocessing

Animals were connected by cable to the recording apparatus via a 32-channel headstage and harness attached to a 40-channel slip-ring commutator (Crist Instruments, Hagerstown, MD) to allow free movement in the behavioral testing chamber. Single neuron action potentials (spikes) were isolated by time-amplitude window discrimination and computer-identified individual waveform characteristics using a multi-neuron acquisition (MAP) processor (Plexon Inc., Dallas, TX, USA). Single neuron spikes were recorded daily and identified using waveform and firing characteristics within the task (perievent histograms) for each of the DNMS events (SR, LNP & NR). To maintain waveform shape

across days, all recorded data was concatenated into one file (separately for each rat) and offline sorting was performed using principal component analysis, peak-valley, and nonlinear energy algorithms in Offline Sorter (Plexon Inc., Dallas, TX, USA). Hippocampal neuron ensembles used to distinguish recording phases and drug treatment conditions consisted of 10-30 single neurons, each recorded from a separate identified electrode location on either of the bilateral arrays. All isolated spike trains contained no less than a 1 ms gap at the center of the autocorrelogram. No effort was made to differentiate between principal cells and interneurons. Previous work has shown that hippocampal neurons recorded with the same waveform from the same electrodes exhibit consistent mean, baseline and DNMS task modulated firing rate alterations [62, 25], and therefore individual neurons were treated as the same when recorded over multiple days. A total of 189 neurons recorded during 5,143 recording phases were analyzed in the reported experiments.

## A.7 Sample-Response Cell Identification

Prior studies from this laboratory have identified hippocampal neurons recorded as above by “Functional Cell Types” (FCTs) described by different behavioral correlates of DNMS task-related events such as lever position and/or phase of the task [25, 24]. Sample-response cells, a subtype of FCTs, were identified by first constructing a smoothed (51 bin) perievent histogram around the sample presentation phase of the DNMS task. The neurons background firing rate mean and variance were calculated from activity 3.5-5s after sample presentation. If the neuron’s MFR from the 2 second window around sample presentation was 4 standard deviations greater than its MFR from the background period it was classified as a sample-response cell. It should be noted that for the purpose of this paper other FCTs such as those which respond to a specific lever (left/right) or trial-type cells were not considered [63].

## A.8 Laguerre Expansion Technique

In order to apply the Laguerre expansion technique [18], the input and output data records were first convolved with the Laguerre functions:

$$v_{x_i}^{(l)} = \sum_{\tau=0}^M b_l(\tau) x_i(t - \tau) \quad (2)$$

$$v_y^{(l)} = \sum_{\tau=0}^M b_l(\tau) y(t - \tau) \quad (3)$$

where  $b_l$  is the  $l^{th}$  Laguerre basis function. By first convolving with the Laguerre basis functions, the dynamical effects of the past input epochs are removed and we are left with a simple regression of contemporaneous data. Substituting the above equations into equation 1, we have:

$$y(t) = k_0 + \sum_{n=1}^N \sum_{l=1}^L c_{l,x_i}(l) v_{l,x_i}(t) + \sum_{l=1}^L c_{l,y}(l) v_{l,y}(t) \quad (4)$$



where  $c_{l,x_i}$  and  $c_{l,y}$  are the feedforward and feedback Laguerre expansion coefficients. To estimate model parameters, eq. 4 was cast in matrix form:

$$\mathbf{y} = \mathbf{V}\mathbf{c} + \epsilon \quad (5)$$

where  $\mathbf{y}$  is the vector of all  $N$  output samples,  $\mathbf{V}$  is the design matrix consisting of the convolved inputs,  $\mathbf{c}$  are the model parameters to be estimated, and  $\epsilon$  is the modeling error. Eq. 5 was solved using least squares regression (LSR). The memory of our system was fixed at 300ms, in accordance with previous studies [59, 64]. The Laguerre parameter  $\alpha$  was fixed at 0.6 to reflect this system memory [18].

## A.9 Model Selection

In theory, the most predictive model would include all recorded inputs. However, such a model would be susceptible to overfitting, and would not reveal which neurons are causally connected to each other. To overcome this issue a forward step-wise selection procedure was used to minimize overfitting and prune out all inputs which are not causally related to the output [65]. Given an output cell and  $M$  potential input cells recorded during the same session, the following steps were used to select the  $N$  input cells which are causally connected to the output cell. First, the data was divided into training (in-sample) and testing (out-of-sample) sets. Then,  $M$  single-input single-output (SISO) models were constructed with each of the potential inputs. The model whose predicted output had the highest correlation, as measured by the Pearson correlation-coefficient,  $\rho$ , with the actual output was selected. Afterwards, N-1 two input models were constructed using the previously selected input and one of the remaining potential inputs. If any of the inputs were able to raise  $\rho$ , the input which raised  $\rho$  the most was selected; otherwise, the procedure was ended, and only 1 input was selected. This procedure was repeated until either none of the inputs were able to raise  $\rho$ , or all  $M$  potential neurons were selected. The  $N$  selected neurons were then used as the model input.

## A.10 Model Validation

To avoid overfitting, Monte Carlo style simulations were used to select those models which represent significant causal connections between input and output neurons and do not just fit noise [66]. The following procedure was used: in each run the real input was randomly permuted with respect to the output. A model was then generated between the permuted input and the real output, and the Pearson correlation coefficient,  $\rho_i$ , was obtained as a metric of performance. T=40 such simulations were conducted for each output and a set of performance metrics,  $\{\rho_i\}_i^T$ , was obtained. Then, using Fisher's transformation, we tested the hypothesis,  $H_0$ , that  $\rho$  was within the population of  $\{\rho_i\}$ . If this hypothesis could be rejected at the 99.99% significance level, the model was deemed significant. The very conservative threshold ( $P < .0001$ ) was used due to the large amount of comparisons being made.

## 595 A.11 Statistical Analysis

596 Unless otherwise noted, the unpaired Mann-Whitney U test was used to assess  
 597 whether significant differences exist between two samples. This test was used  
 598 since it does not assume a normal distribution, and much of our data was found to  
 599 be skewed/nonnormal. Shift estimates (Hodges-Lehman) and confidence inter-  
 600 vals were estimated as prescribed by Higgins [67]. In order to estimate the scale  
 601 estimate, or the ratio between two samples, the data was first log-transformed  
 602 and then scale estimate was taken to be the antilog of the shift estimate. The  
 603  $\chi^2$  test was used to compare proportions.

604 In addition to the Pearson correlation coefficient,  $\rho$ , Receiver Operating Char-  
 605 acteristic (ROC) curves were used to visualize model performance. ROC curves  
 606 plot the true positive rate against the false positive rate over the putative range  
 607 of threshold values for the continuous output,  $y$  [66]. The area under the curve  
 608 (AUC) of ROC plots are used as a performance metric of the model, and have  
 609 been shown to be equivalent to the Mann-Whitney two sample statistic [68].  
 610 The AUC ranges from 0 to 1, with 0.5 indicating a random predictor and higher  
 611 values indicating better model performance. The  $\rho$  and AUC metrics were cho-  
 612 sen as they measure the similarity between a continuous 'prethreshold' signal  
 613 and a spike train. The continuous 'prethreshold' signal was chosen over adding  
 614 a threshold trigger and comparing true output spike train with an output 'post-  
 615 threshold' spike train for two reasons. First, this allows us to avoid specifying the  
 616 threshold trigger value, which relies on the somewhat arbitrary tradeoff between  
 617 true-positive and false-negative spikes [44]. Also, similarity metrics between two  
 618 spike trains often require the specification of a 'binning parameter' to determine  
 619 the temporal resolution of the metric [69, 70].<sup>1</sup>

## 620 B Supplementary Figures

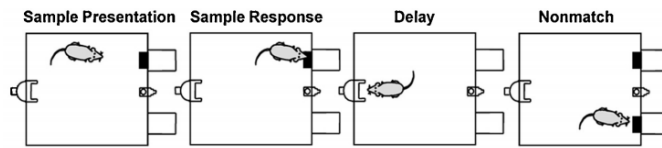


*Figure 6: Schematic of the DNMS task. First the rat is presented with one of two levers (sample presentation), which it presses (sample response). Then following a delay phase, the rat is presented with both levers (Nonmatch), of which it must press the opposite level from which it was presented in order to successfully complete the task.*

<sup>1</sup>I should probably add sections on how behavioral correlation analysis & FFT was done...

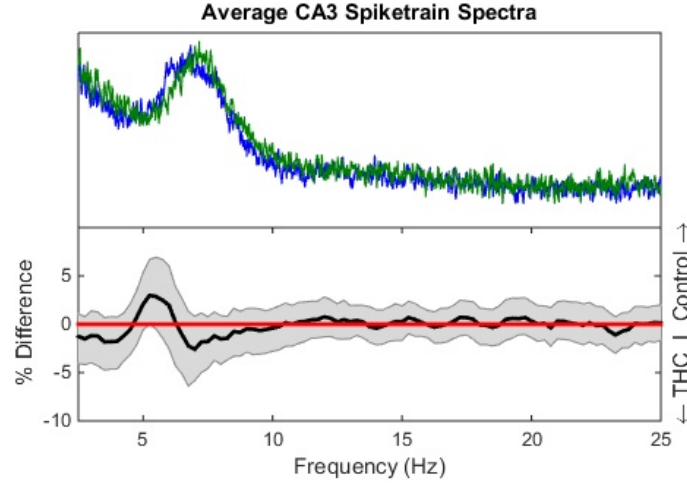


Figure 7: CA3 spectra mean frequency and differences. Same format as Fig. 1e. A weak but significant trend was found for declining CA3 theta oscillations ( $\Delta = 1.94\%$ ,  $P = .045$ ).

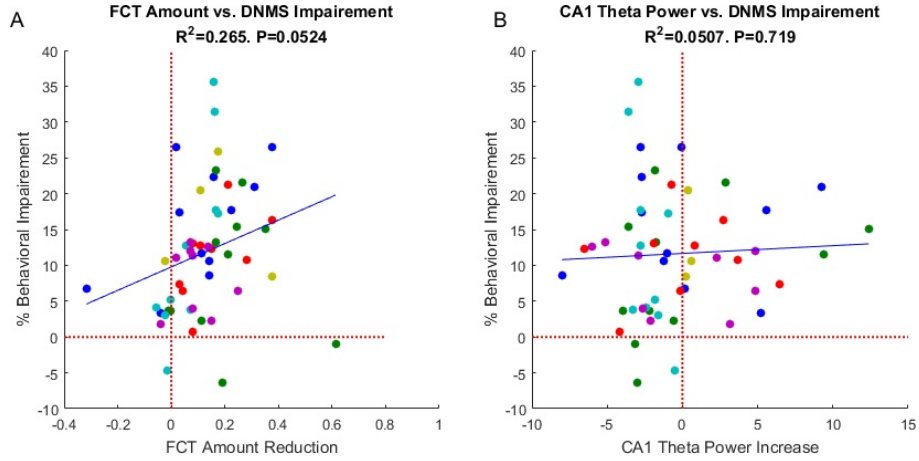


Figure 8: (A) A suggestive but insignificant relationship was found between the THC-induced decrease in the mean number of sample-presentation cells and behavioral performance ( $R^2 = .265$ ,  $P = .052$ ). (B) No relationship was found between reductions in CA1 theta power and behavioral impairment ( $P = .67$ ). Format is same as Fig. 3.

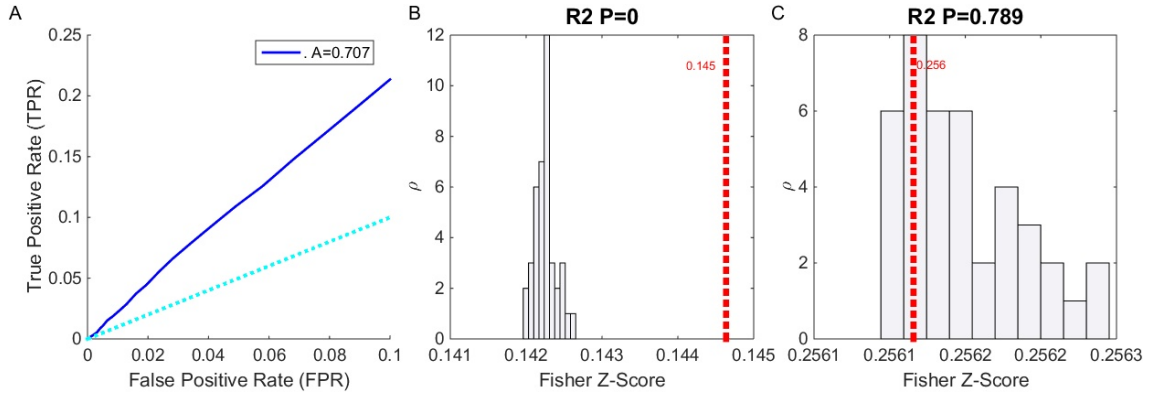


Figure 9: (A) ROC plot (see supplementary methods) for model shown in Fig. 2 showing model predictive power. The light blue line ( $TPR=FPR$ ) indicates a model with no predictive power. (B,C) Examples of Monte Carlo simulations: For each model, 40 surrogate models with shuffled inputs were generated. The Fisher z-scores of these models, which are derived from  $\rho$ , were plotted as a histogram, while the true  $\rho$  value is the plotted dashed red line. The P value for the hypothesis that the true  $\rho$  value is greater than the simulated  $\rho$  values is printed above the graphs. Models were deemed significant if  $P < .0001$ . (B) shows the results for the model in Fig. 2, which was deemed significant. (C) shows an insignificant model

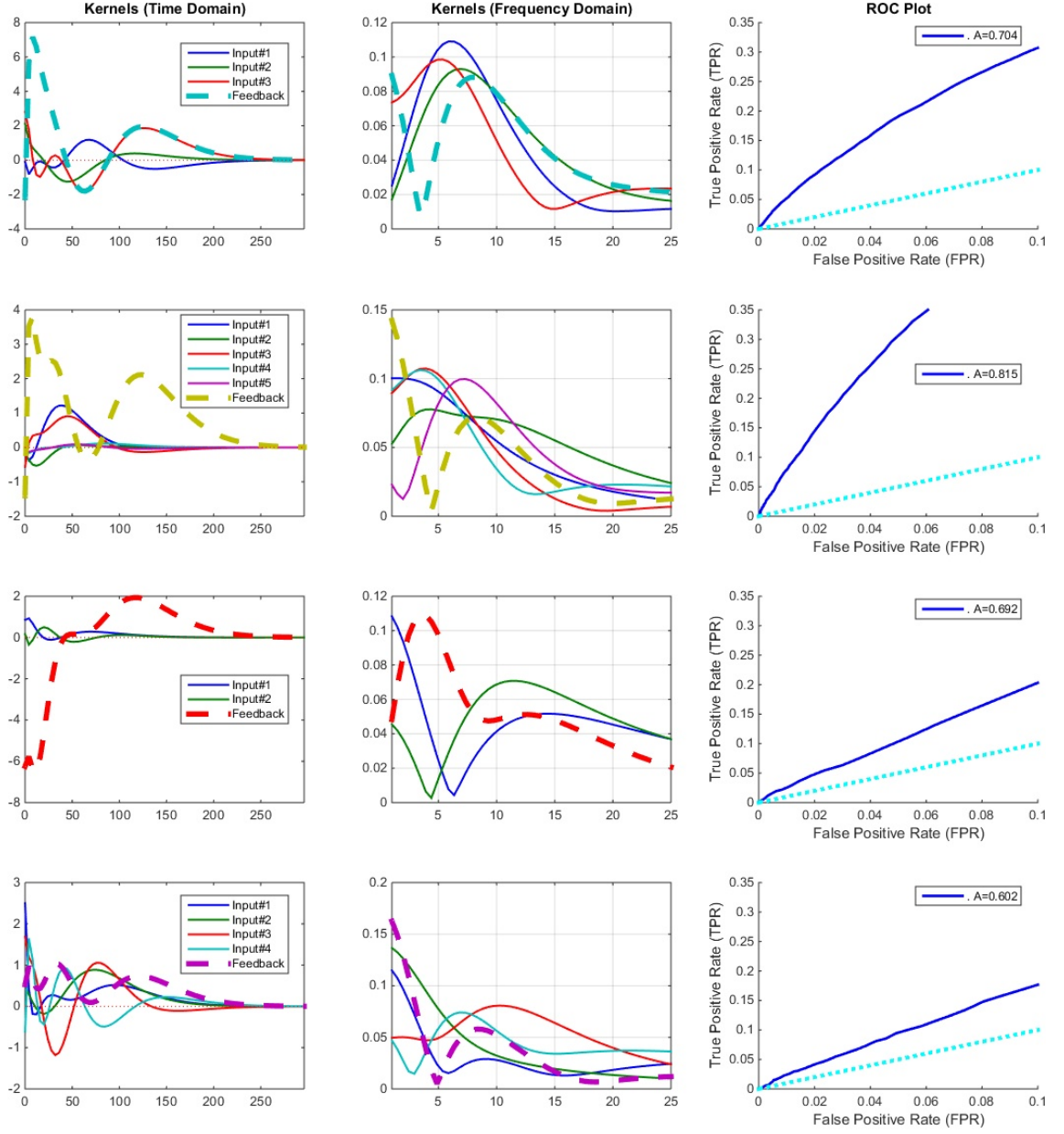


Figure 10: 4 additional systems are presented. Left column shows all system filters, including feedback filter (dashed line) in the time domain. Middle column shows the filters in the frequency domain and right column shows the ROC plots of the models. All these models were found to have significant predictive power in Monte Carlo tests.

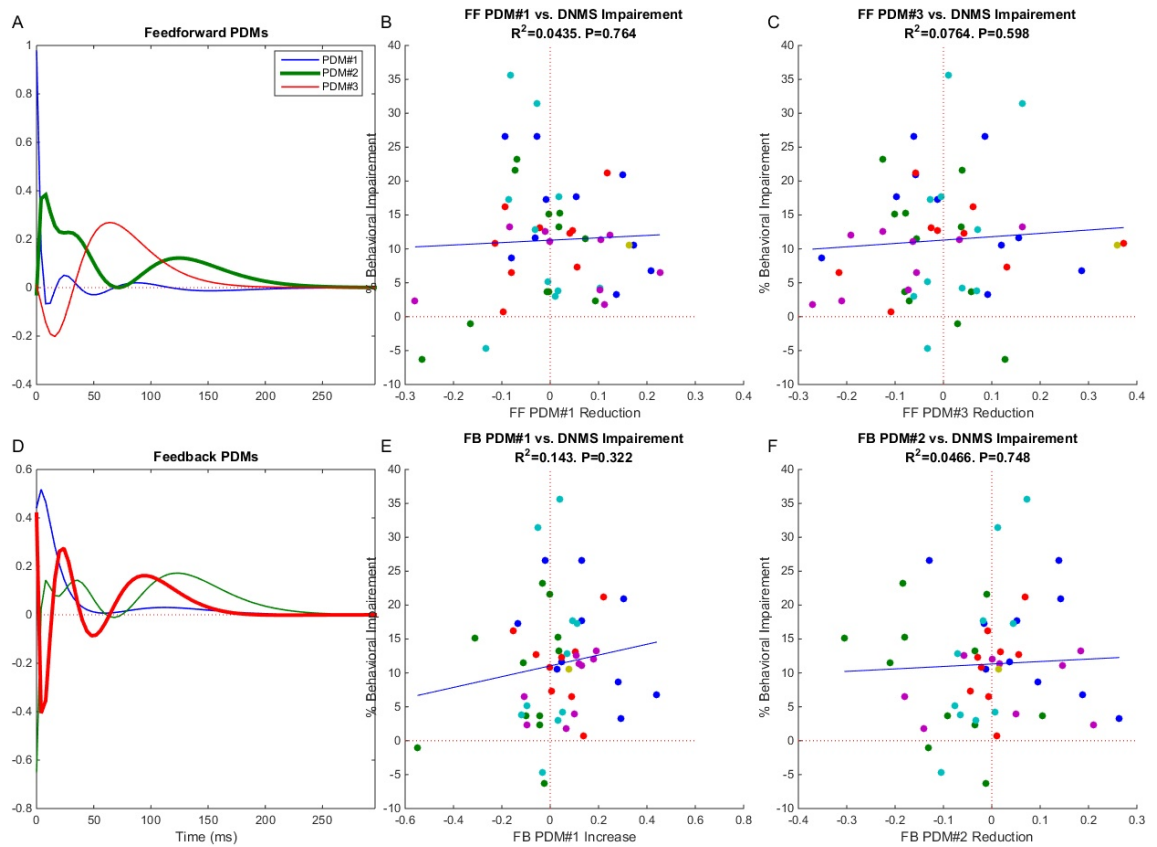


Figure 11: Top Row: neither the first (middle column) nor third feedforward gPDM were found to be significantly correlated with THC induced behavioral deficits. Bottom Row: neither the first (middle column) nor second feedback gPDM were found to be significantly correlated with THC induced behavioral deficits. Format is same as Fig. 3.

## References

- [1] Barbara S Koppel, John CM Brust, Terry Fife, Jeff Bronstein, Sarah Youssof, Gary Gronseth, and David Gloss. Systematic review: Efficacy and safety of medical marijuana in selected neurologic disorders report of the guideline development subcommittee of the american academy of neurology. *Neurology*, 82(17):1556–1563, 2014.
- [2] Liana Fattore. *Cannabinoids in Neurologic and Mental Disease*. Academic Press, 2015.
- [3] Melisa J Wallace, Jenny L Wiley, Billy R Martin, and Robert J DeLorenzo. Assessment of the role of cb 1 receptors in cannabinoid anticonvulsant effects. *European journal of pharmacology*, 428(1):51–57, 2001.
- [4] Robert E Blair, Laxmikant S Deshpande, Sompong Sombati, Katherine W Falenski, Billy R Martin, and Robert J DeLorenzo. Activation of the cannabinoid type-1 receptor mediates the anticonvulsant properties of cannabinoids in the hippocampal neuronal culture models of acquired epilepsy and status epilepticus. *Journal of Pharmacology and Experimental Therapeutics*, 317(3):1072–1078, 2006.
- [5] Laxmikant S Deshpande, Sompong Sombati, Robert E Blair, Dawn S Carter, Billy R Martin, and Robert J DeLorenzo. Cannabinoid cb1 receptor antagonists cause status epilepticus-like activity in the hippocampal neuronal culture model of acquired epilepsy. *Neuroscience letters*, 411(1):11–16, 2007.
- [6] V Rudenko, A Rafiuddin, JR Lehesté, and LK Friedman. Inverse relationship of cannabimimetic (r+) win 55, 212 on behavior and seizure threshold during the juvenile period. *Pharmacology Biochemistry and Behavior*, 100(3):474–484, 2012.
- [7] István Katona. Cannabis and endocannabinoid signaling in epilepsy. In *Endocannabinoids*, pages 285–316. Springer, 2015.
- [8] Andrew J Hill, TD Hill, and B Whalley. The development of cannabinoid based therapies for epilepsy. *Endocannabinoids: molecular, pharmacological, behavioral and clinical features*. bentham science publishers, Oak Park, IL, pages 164–204, 2013.
- [9] Raphael Mechoulam, Lumír O Hanuš, Roger Pertwee, and Allyn C Howlett. Early phytocannabinoid chemistry to endocannabinoids and beyond. *Nature Reviews Neuroscience*, 2014.
- [10] Emma Puighermanal, Arnau Busquets-Garcia, Rafael Maldonado, and Andrés Ozaita. Cellular and intracellular mechanisms involved in the cognitive impairment of cannabinoids. *Philosophical Transactions of the Royal Society B: Biological Sciences*, 367(1607):3254–3263, 2012.

- 660 [11] Mathilde Metna-Laurent and Giovanni Marsicano. Rising stars: Modulation  
661 of brain functions by astroglial type-1 cannabinoid receptors. *Glia*, 63(3):  
662 353–364, 2015.
- 663 [12] Giovanni Bénard, Federico Massa, Nagore Puente, Joana Lourenço, Luigi  
664 Bellocchio, Edgar Soria-Gómez, Isabel Matias, Anna Delamarre, Mathilde  
665 Metna-Laurent, Astrid Cannich, et al. Mitochondrial cb1 receptors regulate  
666 neuronal energy metabolism. *Nature neuroscience*, 15(4):558–564, 2012.
- 667 [13] Wei Xiong, KeJun Cheng, Tanxing Cui, Grzegorz Godlewski, Kenner C  
668 Rice, Yan Xu, and Li Zhang. Cannabinoid potentiation of glycine receptors  
669 contributes to cannabis-induced analgesia. *Nature Chemical Biology*, 7(5):  
670 296–303, 2011.
- 671 [14] Jessica A Fawley, Mackenzie E Hofmann, and Michael C Andresen.  
672 Cannabinoid 1 and transient receptor potential vanilloid 1 receptors dis-  
673 cretely modulate evoked glutamate separately from spontaneous glutamate  
674 transmission. *The Journal of Neuroscience*, 34(24):8324–8332, 2014.
- 675 [15] Moyra A Coull, Andrew T Johnston, Roger G Pertwee, and Stephen N  
676 Davies. Action of  $\delta$ -9-tetrahydrocannabinol on gaba a receptor-mediated  
677 responses in a grease-gap recording preparation of the rat hippocampal slice.  
678 *Neuropharmacology*, 36(10):1387–1392, 1997.
- 679 [16] Timothy M Brown, Jonathan M Brotchie, and Stephen M Fitzjohn.  
680 Cannabinoids decrease corticostriatal synaptic transmission via an effect  
681 on glutamate uptake. *The Journal of neuroscience*, 23(35):11073–11077,  
682 2003.
- 683 [17] Roman A Sandler, Dong Song, Robert E Hampson, Sam A Deadwyler,  
684 Theodore W Berger, and Vasilis Z Marmarelis. Model-based asesment of an  
685 in-vivo predictive relationship from ca1 to ca3 in the rodent hippocampus.  
686 *Journal of computational neuroscience*, pages 1–15, 2014.
- 687 [18] Vasilis Z Marmarelis. *Nonlinear dynamic modeling of physiological systems*.  
688 Wiley-Interscience, 2004.
- 689 [19] Dong Song, Vasilis Z Marmarelis, and Theodore W Berger. Parametric and  
690 non-parametric modeling of short-term synaptic plasticity. part i: Compu-  
691 tational study. *Journal of computational neuroscience*, 26(1):1–19, 2009.
- 692 [20] Dustin Fetterhoff, Ioan Opris, Sean L Simpson, Sam A Deadwyler, Robert E  
693 Hampson, and Robert A Kraft. Multifractal analysis of information pro-  
694 cessing in hippocampal neural ensembles during working memory under  $\delta$   
695 9-tetrahydrocannabinol administration. *Journal of neuroscience methods*,  
696 2014.
- 697 [21] Dustin Fetterhoff, Robert A Kraft, Roman A Sandler, Ioan Opris, Cheryl A  
698 Sexton, Vasilis Z Marmarelis, Robert E Hampson, and Sam A Deadwyler.



- 699 Distinguishing cognitive state with multifractal complexity of hippocampal  
700 interspike interval sequences. *Frontiers in systems neuroscience*, 9, 2015.
- 701 [22] Robert E Hampson and Sam A Deadwyler. Cannabinoids reveal the neces-  
702 sity of hippocampal neural encoding for short-term memory in rats. *The*  
703 *Journal of Neuroscience*, 20(23):8932–8942, 2000.
- 704 [23] David Robbe, Sean M Montgomery, Alexander Thome, Pavel E Rueda-  
705 Orozco, Bruce L McNaughton, and György Buzsáki. Cannabinoids reveal  
706 importance of spike timing coordination in hippocampal function. *Nature*  
707 *neuroscience*, 9(12):1526–1533, 2006.
- 708 [24] Anushka V Goonawardena, Lianne Robinson, Robert E Hampson, and Ger-  
709 not Riedel. Cannabinoid and cholinergic systems interact during perfor-  
710 mance of a short-term memory task in the rat. *Learning & Memory*, 17  
711 (10):502–511, 2010.
- 712 [25] Robert E Hampson, John D Simeral, and Sam A Deadwyler. Distribution  
713 of spatial and nonspatial information in dorsal hippocampus. *Nature*, 402  
714 (6762):610–614, 1999.
- 715 [26] David Robbe and György Buzsáki. Alteration of theta timescale dynamics  
716 of hippocampal place cells by a cannabinoid is associated with memory  
717 impairment. *The Journal of neuroscience*, 29(40):12597–12605, 2009.
- 718 [27] Gyorgy Buzsaki. *Rhythms of the Brain*. Oxford University Press, 2006.
- 719 [28] Laura Lee Colgin. Mechanisms and functions of theta rhythms. *Annual*  
720 *review of neuroscience*, 36:295–312, 2013.
- 721 [29] György Buzsáki and Edvard I Moser. Memory, navigation and theta rhythm  
722 in the hippocampal-entorhinal system. *Nature neuroscience*, 16(2):130–138,  
723 2013.
- 724 [30] James M Hyman, Eric A Zilli, Amanda M Paley, and Michael E Hasselmo.  
725 Working memory performance correlates with prefrontal-hippocampal theta  
726 interactions but not with prefrontal neuron firing rates. *Frontiers in inte-*  
727 *grative neuroscience*, 4, 2010.
- 728 [31] Mihály Hajós, William E Hoffmann, and Bernát Kocsis. Activation of  
729 cannabinoid-1 receptors disrupts sensory gating and neuronal oscillation:  
730 relevance to schizophrenia. *Biological psychiatry*, 63(11):1075–1083, 2008.
- 731 [32] N Spruston and C McBain. Structural and functional properties of hip-  
732 pocampal neurons. *The hippocampus book*, pages 133–201, 2007.
- 733 [33] Thomas Klausberger and Peter Somogyi. Neuronal diversity and temporal  
734 dynamics: the unity of hippocampal circuit operations. *Science*, 321(5885):  
735 53–57, 2008.

- [34] Frédéric Pouille and Massimo Scanziani. Enforcement of temporal fidelity in pyramidal cells by somatic feed-forward inhibition. *Science*, 293(5532):1159–1163, 2001.
- [35] Rita Zemankovics, Judit M Veres, Iris Oren, and Norbert Hájos. Feedforward inhibition underlies the propagation of cholinergically induced gamma oscillations from hippocampal ca3 to ca1. *The Journal of Neuroscience*, 33(30):12337–12351, 2013.
- [36] L Stan Leung and Hui-Wen Yu. Theta-frequency resonance in hippocampal ca1 neurons in vitro demonstrated by sinusoidal current injection. *Journal of neurophysiology*, 79(3):1592–1596, 1998.
- [37] Bruce Hutcheon and Yosef Yarom. Resonance, oscillation and the intrinsic frequency preferences of neurons. *Trends in neurosciences*, 23(5):216–222, 2000.
- [38] Bernat Kocsis, Anatol Bragin, and György Buzsáki. Interdependence of multiple theta generators in the hippocampus: a partial coherence analysis. *The Journal of neuroscience*, 19(14):6200–6212, 1999.
- [39] György Buzsáki. Theta oscillations in the hippocampus. *Neuron*, 33(3):325–340, 2002.
- [40] Romain Goutagny, Jesse Jackson, and Sylvain Williams. Self-generated theta oscillations in the hippocampus. *Nature neuroscience*, 12(12), 2009.
- [41] Krisztina Monory, Martin Polack, Anita Remus, Beat Lutz, and Martin Korte. Cannabinoid cb1 receptor calibrates excitatory synaptic balance in the mouse hippocampus. *The Journal of Neuroscience*, 35(9):3842–3850, 2015.
- [42] SA Turkanis and R Karler. Central excitatory properties of  $\delta$  9-tetrahydrocannabinol and its metabolites in iron-induced epileptic rats. *Neuropharmacology*, 21(1):7–13, 1982.
- [43] Angela B Clement, E Gregory Hawkins, Aron H Lichtman, and Benjamin F Cravatt. Increased seizure susceptibility and proconvulsant activity of anandamide in mice lacking fatty acid amide hydrolase. *The Journal of neuroscience*, 23(9):3916–3923, 2003.
- [44] Vasilis Z Marmarelis, Dae C Shin, Dong Song, Robert E Hampson, Sam A Deadwyler, and Theodore W Berger. Nonlinear modeling of dynamic interactions within neuronal ensembles using principal dynamic modes. *Journal of computational neuroscience*, 34(1):73–87, 2013.
- [45] Roman A Sandler and Vasilis Z. Marmarelis. Understanding spike triggered covariance using wiener theory for receptive field identification. *Journal of Vision*, in press.

- 774 [46] Sam A Deadwyler, James R West, Carl W Cotman, and Gary Lynch. Phys-  
775 iological studies of the reciprocal connections between the hippocampus and  
776 entorhinal cortex. *Experimental neurology*, 49(1):35–57, 1975.
- 777 [47] Roman A Sandler, Dong Song, Robert E Hampson, Sam A Deadwyler,  
778 Theodore W Berger, and Vasilis Z Marmarelis. Closed-loop hippocam-  
779 pal modeling and the design of neurostimulation patterns for suppressing  
780 seizures. *Journal of Neural Engineering*, Under Review.
- 781 [48] Roland SG Jones. Entorhinal-hippocampal connections: a speculative view  
782 of their function. *Trends in neurosciences*, 16(2):58–64, 1993.
- 783 [49] Omar J Ahmed and Mayank R Mehta. The hippocampal rate code:  
784 anatomy, physiology and theory. *Trends in neurosciences*, 32(6):329–338,  
785 2009.
- 786 [50] Roman A Sandler, Samuel A Deadwyler, Robert E Hampson, Dong Song,  
787 Theodore W Berger, and Vasilis Z Marmarelis. System identification of  
788 point-process neural systems using probability based volterra kernels. *Jour-  
789 nal of neuroscience methods*, 240:179–192, 2015.
- 790 [51] Maoxing Shen, Timothy M Piser, Virginia S Seybold, and Stanley A Thayer.  
791 Cannabinoid receptor agonists inhibit glutamatergic synaptic transmission  
792 in rat hippocampal cultures. *The Journal of neuroscience*, 16(14):4322–  
793 4334, 1996.
- 794 [52] Marianne J Bezaire and Ivan Soltesz. Quantitative assessment of ca1 lo-  
795 cal circuits: Knowledge base for interneuron-pyramidal cell connectivity.  
796 *Hippocampus*, 23(9):751–785, 2013.
- 797 [53] I Katona, B Sperlagh, Zs Maglóczy, E Santha, A Köfalvi, S Czirjak,  
798 K Mackie, ES Vizi, and TF Freund. Gabaergic interneurons are the targets  
799 of cannabinoid actions in the human hippocampus. *Neuroscience*, 100(4):  
800 797–804, 2000.
- 801 [54] Robert E Hampson and Sam A Deadwyler. Role of cannabinoid receptors  
802 in memory storage. *Neurobiology of disease*, 5(6):474–482, 1998.
- 803 [55] Miles A Whittington and Roger D Traub.  $i_L$  interneuron diversity se-  
804 ries  $i_L$ : Inhibitory interneurons and network oscillations  $i_L$  in vitro  $i_L$ .  
805 *Trends in neurosciences*, 26(12):676–682, 2003.
- 806 [56] Horacio G Rotstein, Dmitri D Pervouchine, Corey D Acker, Martin J Gillies,  
807 John A White, Eberhardt H Buhl, Miles A Whittington, and Nancy Kopell.  
808 Slow and fast inhibition and an h-current interact to create a theta rhythm  
809 in a model of ca1 interneuron network. *J Neurophysiol*, 94:1509–1518, 2005.
- 810 [57] Can Tao, Guangwei Zhang, Ying Xiong, and Yi Zhou. Functional dissection  
811 of synaptic circuits: in vivo patch-clamp recording in neuroscience. *Frontiers  
812 in Neural Circuits*, 9:23, 2015.

- 813 [58] Vasilis Z Marmarelis, Dae C Shin, Dong Song, Robert E Hampson, Sam A  
814 Deadwyler, and Theodore W Berger. On parsing the neural code in the  
815 prefrontal cortex of primates using principal dynamic modes. *Journal of*  
816 *computational neuroscience*, 36(3):321–337, 2014.
- 817 [59] Dong Song, Rosa HM Chan, Vasilis Z Marmarelis, Robert E Hampson,  
818 Sam A Deadwyler, and Theodore W Berger. Nonlinear dynamic modeling of  
819 spike train transformations for hippocampal-cortical prostheses. *Biomedical*  
820 *Engineering, IEEE Transactions on*, 54(6):1053–1066, 2007.
- 821 [60] George Paxinos and CH Watson. The rat brain in stereotaxic coordi-  
822 nates 2nd edn. *Academic Press, New York. Rasoolijazi, H., Joghataie,*  
823 *MT, Roghani, M., & Nobakht, M.(2007). The beneficial effect of (-)-*  
824 *epigallocatechin-3-gallate in an experimental model of Alzheimer’s disease*  
825 *in rat: a behavioral analysis. Iran Biomed J*, 11(4):237–243, 1986.
- 826 [61] Theodore W Berger, Dong Song, Rosa HM Chan, Vasilis Z Marmarelis, Jeff  
827 LaCoss, Jack Wills, Robert E Hampson, Sam A Deadwyler, and John J  
828 Granacki. A hippocampal cognitive prosthesis: multi-input, multi-output  
829 nonlinear modeling and vlsi implementation. *Neural Systems and Rehabili-*  
830 *tation Engineering, IEEE Transactions on*, 20(2):198–211, 2012.
- 831 [62] Sam A Deadwyler, Terence Bunn, and Robert E Hampson. Hippocampal  
832 ensemble activity during spatial delayed-nonmatch-to-sample performance  
833 in rats. *Journal of Neuroscience*, 16(1):354–372, 1996.
- 834 [63] Robert E Hampson, Dong Song, Rosa HM Chan, Andrew J Sweatt,  
835 Mitchell R Riley, Anushka V Goonawardena, Vasilis Z Marmarelis, Greg A  
836 Gerhardt, Theodore W Berger, and Sam A Deadwyler. Closing the loop  
837 for memory prosthesis: Detecting the role of hippocampal neural ensembles  
838 using nonlinear models. *Neural Systems and Rehabilitation Engineering,*  
839 *IEEE Transactions on*, 20(4):510–525, 2012.
- 840 [64] Ude Lu, Dong Song, and Theodore W Berger. Nonlinear dynamic model-  
841 ing of synaptically driven single hippocampal neuron intracellular activity.  
842 *Biomedical Engineering, IEEE Transactions on*, 58(5):1303–1313, 2011.
- 843 [65] Dong Song, Rosa HM Chan, Vasilis Z Marmarelis, Robert E Hampson,  
844 Sam A Deadwyler, and Theodore W Berger. Nonlinear modeling of neural  
845 population dynamics for hippocampal prostheses. *Neural Networks*, 22(9):  
846 1340–1351, 2009.
- 847 [66] Theodoros P Zanos, Spiros H Courellis, Theodore W Berger, Robert E  
848 Hampson, Sam A Deadwyler, and Vasilis Z Marmarelis. Nonlinear model-  
849 ing of causal interrelationships in neuronal ensembles. *Neural Systems and*  
850 *Rehabilitation Engineering, IEEE Transactions on*, 16(4):336–352, 2008.
- 851 [67] James J. Higgins. *Intoruction to Modern Nonparametric Statistics*. 2003.

- 852 [68] James A Hanley and Barbara J McNeil. The meaning and use of the area  
853 under a receiver operating characteristic (roc) curve. *Radiology*, 143(1):  
854 29–36, 1982.
- 855 [69] Mark CW van Rossum. A novel spike distance. *Neural Computation*, 13  
856 (4):751–763, 2001.
- 857 [70] Jonathan D Victor and Keith P Purpura. Metric-space analysis of spike  
858 trains: theory, algorithms and application. *Network: computation in neural*  
859 *systems*, 8(2):127–164, 1997.